# Deep inelastic scattering data and the problem of saturation in small-*x* physics

A. Capella, E. G. Ferreiro, and C. A. Salgado

*Laboratoire de Physique Théorique, Université de Paris XI, Bâtiment 210, F-91405 Orsay Cedex, France*

A. B. Kaidalov

*ITEP, B. Cheremushkinskaya ulitsa 25, 117259 Moscow, Russia*

We investigate the role of unitarization effects in virtual photon-proton ($\gamma^*p$) interactions at small *x*. The $q\bar{q}$ fluctuation of the initial photon is separated into a small distance and a large distance component and a model for the unitarization of each component is proposed. The Born approximation for the small size component is calculated using QCD perturbation theory. A Reggeon diagram technique is used in order to obtain a self-consistent scheme for both the total $\gamma^*p$ cross section and diffractive production. The model gives a good description of DESY HERA data in the small-*x* region, with a single Pomeron of intercept 1.2.

## I. INTRODUCTION

The present work is an extension of our previous one [1] on the investigation of unitarity effects in small-*x* processes. It was found experimentally at the DESY *ep* collider HERA that both the total cross section of a highly virtual photon, $\sigma_{\gamma^*p}^{(tot)}$, and the cross section for its diffractive dissociation have a fast increase with energy. This is related to a fast increase of densities of quarks and gluons as the Bjorken variable *x* decreases. The dynamics of such very dense partonic systems is very interesting and has been studied by many authors both in deep inelastic scattering (see Ref. [2] for reviews and Ref. [3] for some recent papers) and in high-energy nuclear interactions [4]. Unitarity effects should stop the increase of densities at extremely small *x* and lead to a ''saturation'' of parton densities. It is important to determine the region of *x* and $Q^2$ where the effects of saturation become important.

We study this problem using Reggeon calculus [5] with a supercritical Pomeron [$\alpha_P(0)-1 \equiv \Delta > 0$] and the partonic picture of $\gamma^*p$ interactions in QCD. In our previous paper [1] we used this approach for the description of HERA data in the region $0 \leq Q^2 \leq Q_0^2$ ($Q_0^2 \sim 10 \, \text{GeV}^2$), where the effects of unitarity are most important. It was shown that, with a single Pomeron of intercept 1.2 and multi-Pomeron exchanges (unitarity effects), it is possible to obtain a self-consistent, simultaneous, description of both the total $\gamma^*p$ cross section and diffractive production in high-energy $\gamma^*p$ interactions. In such an approach, it is convenient to consider the process of the $\gamma^*p$ interaction in the laboratory frame as an interaction of the $q\bar{q}$ pair, produced by the photon, with the proton. We separated the $q\bar{q}$-pair fluctuation into two components: and ''aligned'' component, with a strongly asymmetric sharing of the momentum fraction *z* between *q* and $\bar{q}$, and the rest (''symmetric'') component. Such a separation is important at large $Q^2$, where the first component has a large transverse size, while the ''symmetric'' component has a size $r \sim 1/Q$ and thus has a small cross section $\sim 1/Q^2$ of interaction with the target. Both components give a con-

tribution to the $\sigma_{\gamma^*p}^{(tot)}$ which behaves as $1/Q^2$ at large $Q^2$, but the ''aligned'' component gives the main contribution to the diffraction production cross section. Triple-Pomeron diagrams were also included in our model.

In this paper we propose a more direct separation of the two components of the $q\bar{q}$ pair, which is valid also for small $Q^2$. The separation into a small size (*S*) and a large size (*L*) components of the $q\bar{q}$ pair is now made in terms of the transverse distance *r* between *q* and $\bar{q}$. The border value $r_0$ is treated as a free parameter, which turns out to be $r_0 \sim 0.2$ fm.[1]

For the *S* component, with $r \leq r_0$, we use the expression for the $\gamma^*p$ total cross section obtained in perturbative QCD [7,8]:

$$\sigma_{\gamma^*p}^{(tot)T(L)}(s,Q^2) = \int_0^{r_0} d^2r \int_0^1 dz \, |\psi^{T(L)}(r,z,Q)|^2 \sigma_S(r,s,Q^2),$$

$$(1)$$

where *T* and *L* correspond to transverse and longitudinal polarizations of a virtual photon, $\psi^{T(L)}(r,z)$ are the corresponding wave functions of the $q\bar{q}$ pair,

$$|\psi^T(r,z,Q)|^2 = \frac{6\alpha_{e.m.}}{4\pi^2} \sum_q e_q^2 \{[z^2 + (1-z^2)]\epsilon^2 K_1^2(\epsilon r) + m_q^2 K_0^2(\epsilon r)\},$$

$$(2)$$

and

$$|\psi^L(r,z,Q)|^2 = \frac{6\alpha_{e.m.}}{4\pi^2} \sum_q e_q^2 \{4Q^2 z^2 (1-z)^2 K_0^2(\epsilon r)\},$$

$$(3)$$

_____

[1]This value agrees with the correlation length of nonperturbative interactions observed in lattice calculations [6].

with $\epsilon^2 = z(1-z)Q^2 + m_q^2$. Here $K_0$ and $K_1$ are McDonald functions. The sums are over quark flavors and we have taken $m_u = m_d = m_s \equiv m_S$. $\sigma_S(r,s,Q^2)$ is the total cross section for the interaction of the $q\bar{q}$ pair with the proton. For the interaction of a small-size dipole,

$$\sigma_S(r,s,Q^2) = r^2 f(s,Q^2). \quad (4)$$

As for the $L$ component, we use the same parametrizations introduced in Ref. [1] for the aligned component (see Sec. II).

## II. MODEL

We write the $\gamma^*p$ total cross section

$$\sigma_{\gamma^*p}^{(tot)}(s,Q^2) = \frac{4\pi^2 \alpha_{e.m}}{Q^2} F_2(x,Q^2) \quad (5)$$

in the following form, using the impact parameter ($b$) representation:

$$\sigma_{\gamma^*p}^{(tot)}(s,Q^2) = 4 \int d^2b\, \sigma_{\gamma^*p}^{(tot)}(b,s,Q^2), \quad (6)$$

$$\sigma_{\gamma^*p}^{(tot)}(b,s,Q^2) = g_L^2(Q^2)\sigma_L^{(tot)}(b,s,Q^2) + \sigma_S^{(tot)}(b,s,Q^2). \quad (7)$$

The function $g_L^2(Q^2)$ determines the coupling of the photon to the large size $q\bar{q}$ pair and is chosen in the form [1]

$$g_L^2(Q^2) = \frac{g_L^2(0)}{1 + \frac{Q^2}{m_L^2}}, \quad (8)$$

where $g_L^2(0)$ and $m_L^2$ are phenomenological parameters.

The cross section for the $L$ component, $\sigma_L^{(tot)}$, in the impact parameter space, is chosen in the quasieikonal form [1,9]

$$\sigma_L^{(tot)}(b,s,Q^2) = \frac{1 - \exp[-C\chi_L(b,s,Q^2)]}{2C}, \quad (9)$$

$$\chi_L(s,b,Q^2) = \frac{\chi_{L0}^P(b,\xi)}{1 + a\chi_3(s,b,Q^2)} + \chi_{L0}^f(b,\xi). \quad (10)$$

The eikonal functions $\chi_{L0}^k$ ($k = P, f$) are written in a standard Regge form

$$\chi_{L0}^k(b,\xi) = \frac{C_L^k}{\lambda_{0k}^L(\xi)} \exp\left(\Delta_k \xi - \frac{b^2}{4\lambda_{0k}^L(\xi)}\right), \quad (11)$$

where

$$\Delta_k = \alpha_k(0) - 1, \quad \xi = \ln\frac{s + Q^2}{s_0 + Q^2}, \quad \lambda_{0k}^L = R_{0kL}^2 + \alpha_k'\xi. \quad (12)$$

TABLE I. Values of the parameters in the model.

| Fixed parameters | | Fitted parameters | |
|---|---|---|---|
| $\Delta_P$ | 0.2 | $g_L^2(0)$ | $4.56 \times 10^{-3}$ |
| $\Delta_f$ | $-0.3$ | $C_L^f$ | 1.97 GeV$^{-2}$ |
| $\alpha_P'$ | 0.25 GeV$^{-2}$ | $C_L^P$ | 0.56 GeV$^{-2}$ |
| $\alpha_f'$ | 0.9 GeV$^{-2}$ | $s_0$ | 0.79 GeV$^2$ |
| $R_{0kL}^2$ | 3 GeV$^{-2}$ | $a$ | $4.63 \times 10^{-2}$ GeV$^{-2}$ |
| $R_{0PS}^2$ | 2 GeV$^{-2}$ | $m_L^2$ | 0.59 GeV$^2$ |
| $R_{1k}^2$ | 2.2 GeV$^{-2}$ | $C_S$ | 0.18 |
| $\gamma_f$ | 8 | $r_0$ | 1.06 GeV$^{-1}$ |
| $C$ | 1.5 | $m_S^2$ | 0.15 GeV$^2$ |

Here $\alpha_k(0)$ is the intercept of the trajectory $k$ and $\alpha_k'$ its slope. The values of the radii $R_{0kL}^2$, based on Ref. [10], are given in Table I. The quantity $\xi$ is chosen in such a way as to behave as $\ln(1/x)$ for large $Q^2$ and as $\ln(s/s_0)$ for $Q^2 = 0$.

The coefficients $C_L^P$ and $C_L^f$ determine, respectively, the residues of the Pomeron and $f$-Reggeon exchanges in the $q\bar{q}$-proton interaction. The coefficient $C = 1.5$ takes into account the dissociation of a proton [9].

We turn next to the denominator of Eq. (10). The constant $a$ is given by $a = g_{pp}^P(0)r_{PPP}(0)/16\pi$, where $g_{pp}^P(0)$ is the proton-Pomeron coupling and $r_{PPP}(0)$ is the triple-Pomeron coupling, both at $t = 0$. The function $\chi_3(b,s,Q^2)$ is given by Eq. (31) of Sec. III.

With $a = 0$, the model described above is a standard quasieikonal model with a Born term given by Pomeron plus $f$ exchanges. The denominator in Eq. (10) corresponds to a resummation of triple-Pomeron branchings (the so-called fan diagrams). (For a full discussion of the interpretation of this denominator see Ref. [1].) Thus, expressions (9) and (10) correspond to a sum of diagrams of the type shown in Fig. 1.

We turn next to the $S$ component. In this case we put, in complete analogy with Eqs. (9)–(11),

$$\sigma_S^{(tot)}(r,b,s,Q^2) = \frac{1 - \exp[-C\chi_S(r,b,s,Q^2)]}{2C}, \quad (13)$$

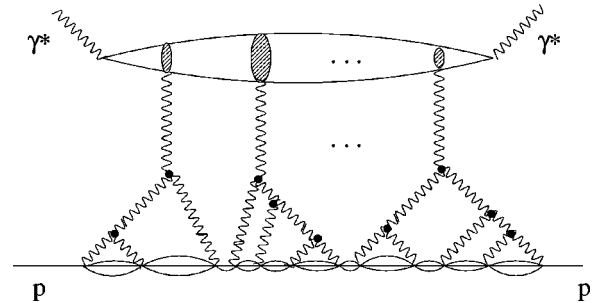$$\chi_S(r,b,s,Q^2) = \frac{\chi_{S0}(r,b,s,Q^2)}{1 + a\chi_3(b,s,Q^2)}, \quad (14)$$



FIG. 1. A generic Reggeon diagram of our model. It contains the $s$-channel iteration of Pomeron and $f$ exchanges, triple-Pomeron ($PPP + PfP$) diagrams, as well as multiple $t$-channel branchings of the Pomeron of the fan-diagram type.

$$\chi_{S0}(r,b,\xi)=\frac{C_S^P r^2}{\lambda_{0P}^S(\xi)}\exp\left(\Delta_P\xi-\frac{b^2}{4\lambda_{0P}^S(\xi)}\right),$$

(15)

with $\lambda_{0P}^S=R_{0PS}^2+\alpha_P'\xi$.

Note that the contribution of the $f$ exchange to the $S$ component is very small and has been neglected [1]. The condition (4), valid for fixed $s$ and $Q^2$ as $r\rightarrow 0$, is a property of the single Pomeron exchange. Thus a factor $r^2$ has been introduced in Eq. (15).

Finally $\sigma_S(r,s,Q^2)$ in Eq. (1) is obtained from $\sigma_S(r,b,s,Q^2)$, defined by Eqs. (13)–(15), as [see Eq. (6)]

$$\sigma_S(r,s,Q^2)=4\int d^2b\,\sigma_S(r,b,s,Q^2).$$

(16)

Inserting this expression in Eq. (1) we obtain the transverse and longitudinal contributions of the $S$ component to the total $\gamma^*p$ cross section.

## III. DIFFRACTIVE PRODUCTION

Following Ref. [1] we express the total diffractive dissociation cross section of a virtual photon as a sum of three terms:

$$\sigma_{\gamma^*p}^{(diff)}=\sum_{i=L,S}\sigma_i^{(0)}+\sigma_{PPP},$$

(17)

where

$$\sigma_L^{(0)}=4g_L^2(Q^2)\int(\sigma_L^{(tot)}(b,s,Q^2))^2d^2b,$$

(18)

$$\sigma_S^{(0)T,L}=4\int d^2b\int_0^{r_0}d^2r\int_0^1 dz|\psi^{T,L}(z,r)|^2$$

$$\times[\sigma_S^{tot}(r,b,s,Q^2)]^2,$$

(19)

$$\sigma_{PPP}=2g_L^2(Q^2)\int\chi_{PPP}^L(b,s,Q^2)e^{-2C\chi_L(b,s,Q^2)}d^2b$$

$$+2\int d^2b\int_0^{r_0^2}d^2r\int_0^1 dz\sum_{T,L}|\psi^{T,L}(z,r)|^2$$

$$\times\chi_{PPP}^S(b,s,Q^2)e^{-2C\chi_S(r,b,s,Q^2)}.$$

(20)

Here

$$\chi_{PPP}^L(b,s,Q^2)=a\chi_L^P(b,s,Q^2)\chi_3(b,s,Q^2)$$

(21)

and

$$\chi_{PPP}^S(r,b,s,Q^2)=a\chi_S(r,b,s,Q^2)\chi_3(b,s,Q^2),$$

(22)

where $\chi_L^P(b,s,Q^2)$ is given by the first term of Eq. (10) and $\chi_3(b,s,Q^2)$ is defined by Eq. (31). Using this expression, we see that, to first order in $a$, $\sigma_{PPP}$ consists of the sum of a triple Pomeron ($PPP$) term plus a $PfP$ one. We call this sum triple-Pomeron, although the second one is an interfer-ence term. For the total diffractive production cross section, which includes the diffraction dissociation of a proton, Eqs. (18)–(20) must be multiplied by the same factor $C=1.5$ as in the total $\gamma^*p$ cross section.

At HERA, differential diffractive cross sections are given as a function of $\beta=Q^2/(M^2+Q^2)$, where $M$ is the mass of the diffractively produced system or of $x_P=x/\beta$. They are usually integrated over $t$, and the function $F_{2D}^{(3)}$ is introduced:

$$x_PF_{2D}^{(3)}=\frac{Q^2}{4\pi^2\alpha_{e.m.}}\int x_P\frac{d\sigma}{dx_Pdt}dt.$$

(23)

In our model, this function can be written as a sum of three terms:

$$F_{2D}^{(3)}=\left(\sum_{i=L,S}F_{2Di}^{(3)}(x,Q^2,\beta)+F_{2DPPP}^{(3)}(x,Q^2,\beta)\right).$$

(24)

Here

$$x_PF_{2DL}^{(3)}=\frac{Q^2g_L^2(Q^2)}{4\pi\alpha_{e.m.}}\frac{\sigma_L^{(0)}}{\sigma_L^{(0)B}}\sum_{i,k=P,f}\int d^2b\chi_L^i\chi_L^k$$

$$\times\frac{\widetilde{\beta}^{\Delta_i+\Delta_k-\Delta_f}(1-\beta)^{n_P(Q^2)}}{\displaystyle\int_{\beta_{min}}^{\beta_{max}}\frac{d\beta}{\beta}\widetilde{\beta}^{\Delta_i+\Delta_k-\Delta_f}(1-\beta)^{n_P(Q^2)}}$$

(25)

and

$$x_PF_{2DS}^{(3)}=\frac{Q^2}{4\pi\alpha_{e.m.}}\left(\sigma_S^{(0)T}\frac{\widetilde{\beta}^3(1-2\beta)^2}{\displaystyle\int_{\beta_{min}}^{\beta_{max}}\frac{d\beta}{\beta}\widetilde{\beta}^3(1-2\beta)^2}\right.$$

$$\left.+\sigma_S^{(0)L}\frac{\widetilde{\beta}^3(1-\beta)}{\displaystyle\int_{\beta_{min}}^{\beta_{max}}\frac{d\beta}{\beta}\widetilde{\beta}^3(1-\beta)}\right),$$

(26)

where $\widetilde{\beta}=(Q^2+s_0)/(Q^2+M^2)$, $\beta_{min}=x/x_P^{max}=10x$, and $\beta_{max}=Q^2/(M_{min}^2+Q^2)$ with $M_{min}^2=4m_\pi^2$. In Eq. (25), $\sigma_L^{(0)B}$ corresponds to Eq. (18), keeping only the linear term in $\sigma_L^{(tot)}$, and $\chi_L^{P(f)}$ is the contribution of the $P(f)$ in Eq. (10).

The $\beta$ dependence of the $S$ component has been taken from the QCD results of Ref. [11]. The $\beta$ dependence of the $L$ component was chosen according to Ref. [12] with

$$n_P(Q^2)=-\frac{1}{2}+\frac{3}{2}\left(\frac{Q^2}{c+Q^2}\right),$$

(27)

and $c=3.5\,\text{GeV}^2$.

The triple-Pomeron (i.e., $PPP$ plus $PfP$) contribution $F_{2DPPP}^{(3)}(x,Q^2,\beta)$ is given by

$$x_PF_{2DPPP}^{(3)}(x,Q^2,\beta)=x_PF_{2DPPP}^{(3)B}(x,Q^2,\beta)\frac{\sigma_{PPP}}{\sigma_{PPP}^B},$$

(28)

where $\sigma_{PPP}$ is given by Eq. (20), its Born term $\sigma^B_{PPP}$ by the same equation with $C=0$, and

$$x_P F^{(3)B}_{2DPPP}(x,Q^2,\beta)$$

$$= \frac{Q^2}{4\pi^2 \alpha_{e.m.}} 2a \int d^2b \chi_3(b,s,Q^2,\beta)$$

$$\times \left\{ g_L^2(Q^2)\chi_L^P(b,s,Q^2) \right.$$

$$\left. + \sum_{T,L} \int_0^{r_0} d^2r \int_0^1 dz |\psi^{T,L}(r,z)|^2 \chi_S(r,b,s,Q^2) \right\}. \quad (29)$$

Here

$$\chi_3(s,b,Q^2,\beta) = \sum_{k=P,f} \gamma_k \exp\left( -\frac{b^2}{4\lambda_k\left(\frac{\tilde{\beta}}{\tilde{x}}\right)} \right)$$

$$\times \left(\frac{\tilde{\beta}}{\tilde{x}}\right)^{\Delta_k} \frac{(1-\beta)^{n_P(Q^2)+4}}{\lambda_k\left(\frac{\tilde{\beta}}{\tilde{x}}\right)}, \quad (30)$$

where $\gamma_P = 1$, $\gamma_f$ determines the strength of the $PfP$ contribution relative to the $PPP$ one, and $\lambda_k = R_{1k}^2 + \alpha'_k \ln(\tilde{\beta}/\tilde{x})$. The function $\chi_3(s,b,Q^2)$, which enters in Eqs. (10), (14), (21), and (22), is given by

$$\chi_3(s,b,Q^2) = \int_{\beta_{min}}^{\beta^{max}} \frac{d\beta}{\beta} \chi_3(s,b,Q^2,\beta). \quad (31)$$

Since the triple-Pomeron formula is not valid for low masses, we use here $M_{min}=1$ GeV.

## IV. COMPARISON WITH EXPERIMENTS

The model was used to perform a fit of the data on structure function $F_2(x,Q^2)$ and diffractive structure function $F_{2D}^{(3)}(x,Q^2,\beta)$, in the region of small $x$ ($x<10^{-2}$) and $Q^2 \lesssim 10$ GeV$^2$. More precisely, for $F_2$ we have only included in the fit data up to $Q^2 \lesssim 3.5$ GeV$^2$. For higher values of $Q^2$, QCD evolution is important and is not included in the model. Nevertheless, our parametrization describes the data up to higher values of $Q^2$. For $F_{2D}$ we have included data up to $Q^2 = 18$ GeV$^2$. However, for the higher values of $Q^2$ we have only included data at intermediate values of $\beta$, where the effects of QCD evolution are rather small. At small $\beta$ these effects become large and our parametrization starts to deviate from the data at $Q^2 \gtrsim 18$ GeV$^2$. In Table I, the full list of parameters (fitted and fixed) is given. The overall value of $\chi^2$ is 400 for a total of 273 data points. For $F_{2D}$ the $\chi^2$ is very good—99 for 96 data points. For $F_2$ it is worse—302 for 186 data points. The latter seems to be due to the fact that SLAC data and HERA data are taken together. Using each set of data separately the $\chi^2/N_{DF}$ would be very close to unity.
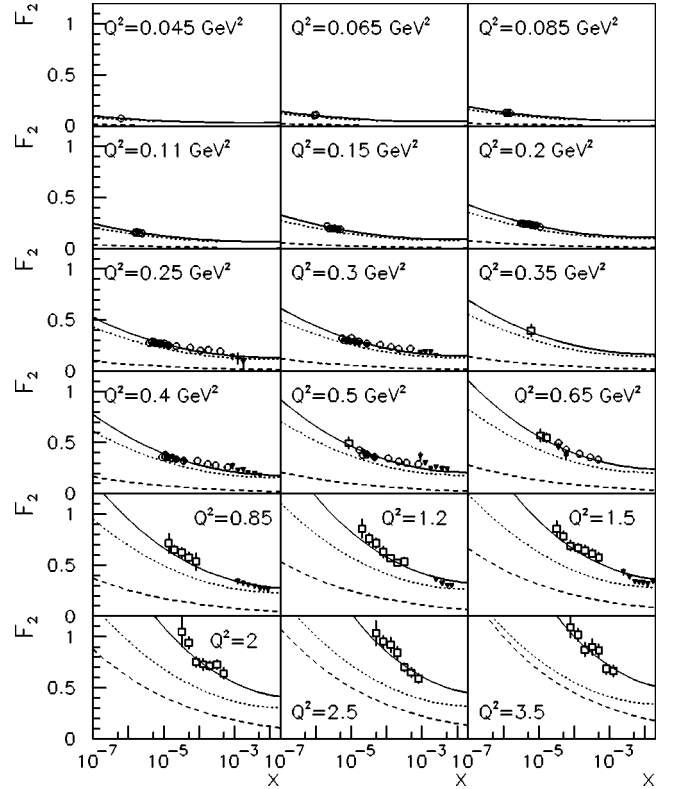


FIG. 2. $F_2(x,Q^2)$ as a function of $x$ for different values of $Q^2$ compared with experimental data from H1 1995 [16] (open squares), ZEUS 1995 [17] (solid circles), E665 [18] (solid triangles) (notice that the corresponding $Q^2$ values of these data are slightly different), and ZEUS BPT97 [19] (open circles). The dotted curve corresponds to the $L$ contribution, the dashed one to the $S$ contribution, and the solid one to the total $F_2(x,Q^2)$ given by the model.

In Fig. 2, the results for $F_2(x,Q^2)$ are given as a function of $x$ for different values of $Q^2$. The description of the data is good. $S$ and $L$ contributions are shown separately in order to see the different behaviors. The $S$ contribution is almost negligible for very small $Q^2$, becoming comparable to the $L$ one at larger $Q^2$ values.

In Figs. 3–6 we compare the model with the experimental data on diffraction. In order to do such a comparison, it is necessary to take into account that different experiments use slightly different definitions of diffractive events. In this way we have multiplied Eqs. (18)–(20) by a factor $C_{diff}=1.1$ in order to compare with data from H1 experiment and $C_{diff} = 1.3$ for ZEUS.[2] With these factors we take into account the different cuts in the mass of the system produced in the diffractive dissociation of the proton (which is larger in the case of ZEUS). In Figs. 3–6, $L$, $S$, and $PPP$ contributions are plotted separately. In Fig. 3, we show our results for the $\beta$ dependence of $x_P F_{2D}^{(3)}$ for $x_P=0.003$ and for two values of $Q^2$. In Fig. 4, the results are given as a function of $x_P$ for

_____

[2] Notice that we have taken these values as constant for each experiment, though they could also depend on $M$. This would improve the agreement in Fig. 5(a).
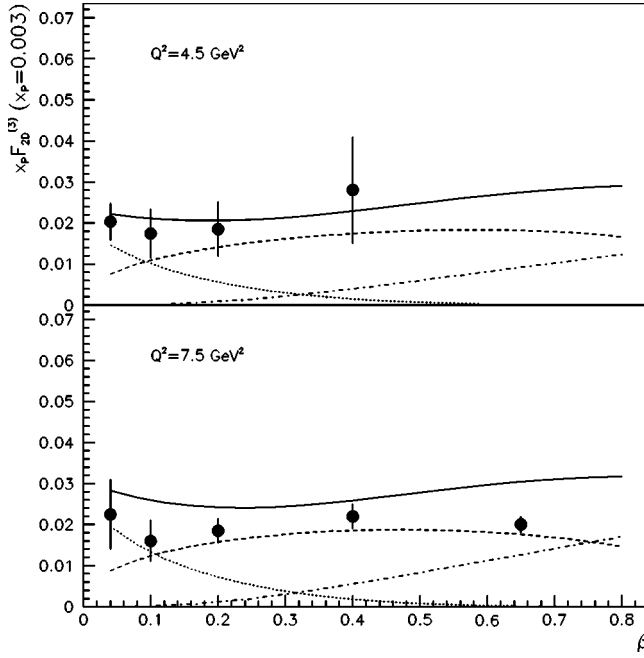
FIG. 3. $x_P F_{2D}^{(3)}$ as a function of $\beta$ for fixed $x_P = 0.003$ and for $Q^2 = 4.5$ GeV$^2$ and $Q^2 = 7.5$ GeV$^2$. Experimental data are from [20]. Dotted lines correspond to the $PPP$ contribution, dashed ones to the $L$ term, and dot-dashed ones to the $S$ one.

different values of $\beta$ and $Q^2$. For the highest values of $Q^2$, only comparison with $\beta = 0.4$ and $\beta = 0.65$ are given. For smaller values of $\beta$, QCD evolution becomes important. In Fig. 5, the energy dependence of the diffraction cross section is shown for different values of $M$ and $Q^2$. In Fig. 6, the $M^2$ dependence for diffractive dissociation in photoproduction is compared with HERA data for two different energies. Only data with $M^2 < 100$ GeV$^2$ are shown for comparison. For larger values, the effect of the nondiffractive $RRP$ contribution (not included in the model) is expected to be large.

As seen in Table I, our fit contains nine free parameters—with which we describe a two-variable function $F_2$ and a three-variable one $F_{2D}$. However, in our opinion, the important feature of our analysis is that it gives a common description of $F_2$ and $F_{2D}$ in a rather broad range of $Q^2$ (including $Q^2 = 0$) with a single Pomeron. Moreover, we describe soft and hard diffraction with the same triple-Pomeron coupling. Furthermore, the values of the parameters are physically very reasonable and amazingly close to the ones expected from hadronic data as we are going to discuss below. We have already commented on the value of $r_0$. As for $s_0 \approx 1$ GeV$^2$ it is the usual value in Regge fits. $m_S \approx 0.35$ GeV$^2$ is the standard value of the mass for a constituent quark and $m_L$ is very close to the mass of $\rho$ meson. Very important parameters in our model are $g_L$, $C_L$, $C_S$, and $a$. We see from Eq. (7) that $g_L \sim \sigma^{\gamma p}/\sigma^{\pi p} (\sim \sigma^{\gamma p}/\sigma^{pp}) \sim 4.5 \times 10^{-3}$ in ideal agreement with the result of our fit. Since vector meson dominance works well at $Q^2 = 0$, it is no wonder that the cross section for our large component (controlled by the parameter $C_L$) is close at $Q^2 = 0$ to $\sigma^{\pi p}$. The constant $C_S$ determines the cross section of the small-size component which can be computed in perturbative QCD. Within large uncertainties, as a result
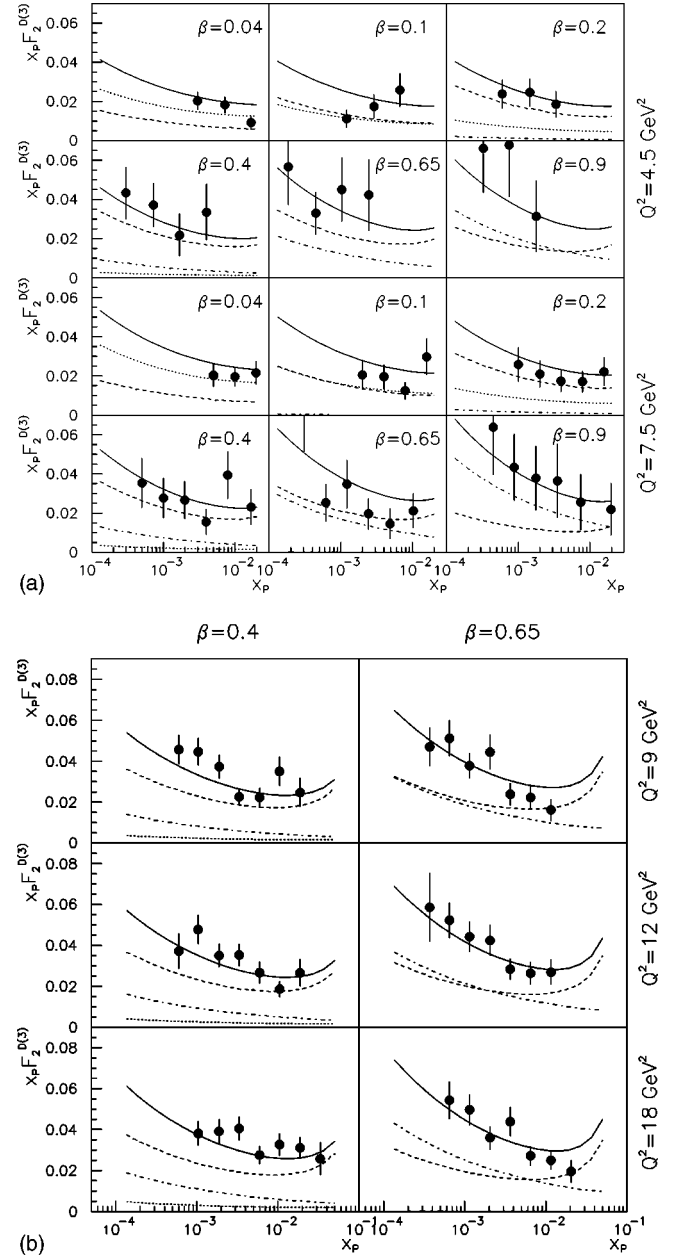


FIG. 4. (a) $x_P F_{2D}^{(3)}$ as a function of $x_P$ for $Q^2 = 4.5$ and 7.5 GeV$^2$ and fixed $\beta = 0.04$, 0.1, 0.2, 0.4, 0.65, and 0.9. The curves are labeled as in Fig. 3. Experimental data are from [20]. (b) $x_P F_{2D}^{(3)}$ as a function of $x_P$ for $Q^2 = 9$, 12, and 18 GeV$^2$ and fixed $\beta = 0.4$ and 0.65. The curves are labeled as in Fig. 3. Experimental data are from [20].

of the poor knowledge of the gluon distributions at small $Q^2$, the value of our parameter is consistent with the QCD calculation. As for the value of $a$, the result of the fit is consistent with the value obtained in Ref. [15] from hadronic data. (Note that $a$ does not contain the coupling to the virtual photon and therefore it is obviously the same for the $L$ and $S$ components.) Finally, the value 1.2 of the Pomeron intercept was obtained in [15] from an analysis of hadronic data and has been fixed. However, we have also tried to leave it as a free parameter and the obtained value is very close to 1.2.
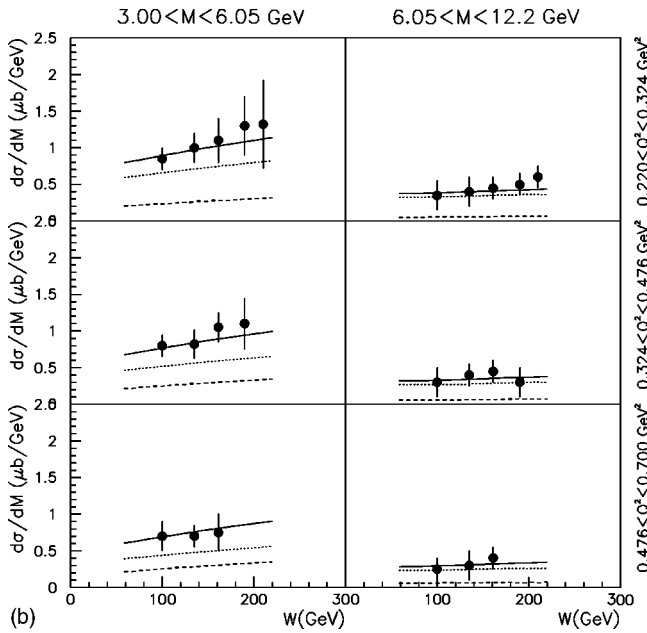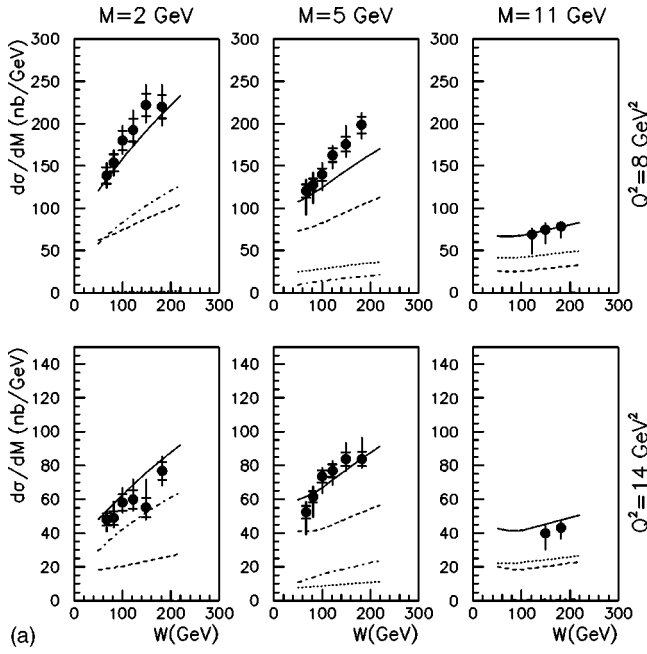
(a)



(b)

FIG. 5. (a) Energy dependence of diffractive cross section for $M = 2$, 5, and 11 GeV and $Q^2 = 8$ and 14 GeV$^2$. Experimental data are from [21]. The curves are labeled as in Fig. 3. (b) Energy dependence of diffractive cross section for different mass intervals and for low $Q^2$ compared with experimental data from [22]. The curves are labeled as in Fig. 3.

## V. CONCLUSIONS

We have introduced a model of the eikonal type to describe total and diffractive $\gamma^* p$ interactions. The $\gamma^* p$ interaction is viewed as that of a $q\bar{q}$ pair, produced by the virtual photon, with the proton. The $\gamma^* p$ total cross section is separated into two components: large size ($L$) for $r > r_0$ and small size ($S$) for $r < r_0$, where $r$ is the transverse distance between
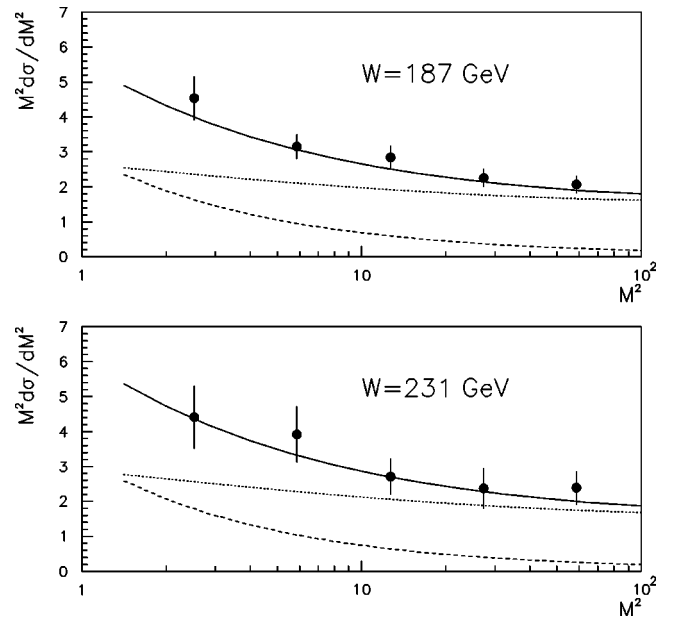


FIG. 6. Diffractive photoproduction cross section for $W = 187$ and 231 GeV as a function of $M^2$ from [23] compared with our model. The curves are labeled as in Fig. 3.

$q$ and $\bar{q}$. The value of $r_0$—treated as a free parameter—turns out to be $r_0 \sim 0.2$ fm. For the $L$ component, all the $Q^2$ dependence is given by the coupling of $\gamma^*$ to the large size $q\bar{q}$ pair—which is taken as $1/Q^2$ at large $Q^2$ [Eq. (8)]. For the $S$ component, the $Q^2$ dependence is given by the wave function of the $q\bar{q}$ pair [Eqs. (2),(3)], computed in perturbative QCD. At large $Q^2$, $r^2 \sim 1/Q^2$, and the unitarity corrections of the $S$ component are higher twist, whereas those of the $L$ have the same $Q^2$ dependence as the Born term—and thus are dominant at large $Q^2$.

A good description of the small-$x$ data is obtained both for $F_2$ and diffractive production, in a broad region of $Q^2$ ($0 \leq Q^2 \lesssim 10$ GeV$^2$), with a single Pomeron of intercept $\alpha_P(0) = 1.2$. For larger values of $Q^2$, QCD evolution becomes important. In particular it gives rise to a behavior $F_2 \sim x^{-\Delta}$ with $\Delta$ significantly larger than 0.2 at large $Q^2$ [13]. For diffraction, this evolution has rather small effects at intermediate values of $\beta$ [14]. This allows us to use our model, in this case without QCD evolution, up to rather large $Q^2$ and moderate $\beta$.

In the region $0 \leq Q^2 \leq 10$ GeV$^2$ the unitarity effects are very important and produce a significant decrease of the effective Pomeron intercept $\alpha_P(0) = 1 + \Delta_P$ with decreasing $Q^2$. This decrease is controlled by the strength of the unitarity corrections. This, in turn, is controlled by the ratio $\sigma^{(diff)}/\sigma^{(tot)}$ and its dependence on $Q^2$. Hence the importance of describing both total cross sections and diffractive production. In our case, $\chi_L > \chi_S$ and the unitarity corrections are more important in the $L$ component than in the $S$. Moreover, these corrections are higher twist at large $Q^2$ in the second case. This is more clearly seen in diffraction, where the $S$ contribution to $x_P F_{2D}^{(3)}(x, Q^2, \beta)$ is much smaller than the $L$ one for all but the larger $\beta$ values.

An important result of our analysis is not only the fact

that we can describe the data on both structure function and diffractive production in a broad region of $Q^2$ with a single Pomeron, but also that we can describe diffractive production at $Q^2 = 0$ and at intermediate $Q^2$ using the same value of the triple-Pomeron coupling (which appears in our parameter $a$).

Finally, we would like to discuss the large $\ln(1/x)$ limit of the total $\gamma^* p$ cross section in our model. The $\sigma_L^{(tot)}(b, s, Q^2)$, given by Eqs. (9)–(11), tends to saturate fastly with increasing $s$ to the value $1/2C$, due to the large $\chi_L(s, b, Q^2)$. The situation is different for the $S$ component. Let us forget for the moment about the triple-Pomeron contribution, i.e., consider the case $a = 0$. As we have said, unitarity corrections are much smaller in the $S$ component, so saturation will take place at much higher energies, when the $\exp(\xi \Delta_P)$ term becomes large enough. For such energies, the cross section in the small impact parameter region will saturate to a $Q^2$-independent value and $F_2(x, Q^2) \sim Q^2$. This is the usual picture in perturbative QCD [2–4]. However, by including the nonperturbative (large distance) $PPP$ terms ($a \neq 0$) we obtain a different behavior. Indeed, the large $\exp(\xi \Delta_P)$ factors in the numerator and denominator of Eq. (14) cancel with each other, and we have $\sigma_{\gamma^* p}^{(tot)} \sim (1/Q^2) f(\ln Q^2)$. Thus, the $1/Q^2$ smallness of the $\gamma^* p$ cross section is maintained in the limit $x \to 0$.

[1] A. Capella, E. G. Ferreiro, A. Kaidalov, and C. A. Salgado, Nucl. Phys. **B593**, 336 (2001).

[2] L. V. Gribov, E. M. Levin, and M. G. Ryskin, Phys. Rep. **100**, 1 (1983); E. Laenen and E. Levin, Annu. Rev. Nucl. Part. Sci. **44**, 199 (1994); A. B. Kaidalov, Surv. High Energy Phys. **9**, 143 (1996); A. H. Mueller, hep-ph/9911289.

[3] A. H. Mueller, Nucl. Phys. **B437**, 107 (1995); A. L. Ayala, M. B. Gay Ducati, and E. M. Levin, Phys. Lett. B **388**, 188 (1996); Nucl. Phys. **B493**, 305 (1997); **B510**, 355 (1998); E. Gotsman, E. Levin, and U. Maor, *ibid.* **B493**, 354 (1997); Phys. Lett. B **425**, 369 (1998); **452**, 387 (1999); E. Gotsman, E. Levin, U. Maor, and E. Naftali, Nucl. Phys. **B539**, 535 (1999); L. L. Frankfurt, W. Kopf, and M. Strikman, Phys. Rev. D **57**, 512 (1998); **54**, 3194 (1996); M. MacDermott, L. L. Frankfurt, V. Guzey, and M. Strikman, hep-ph/9912547; K. Golec-Biernat and M. Wüsthoff, Phys. Rev. D **59**, 014017 (1999); **60**, 114023 (1999); A. H. Mueller, Eur. Phys. J. A **1**, 19 (1998).

[4] L. McLerran and R. Venugopalan, Phys. Rev. D **49**, 2233 (1994); **49**, 3352 (1994); **50**, 2225 (1994); **53**, 458 (1996); J. Jalilian-Marian *et al.*, *ibid.* **59**, 014014 (1999); **59**, 034007 (1999); A. Kovner, L. McLerran, and H. Weigert, *ibid.* **52**, 3809 (1995); **52**, 6231 (1995); Yu. V. Kovchegov and A. H. Mueller, Nucl. Phys. **B529**, 451 (1998); Yu. V. Kovchegov, A. H. Mueller, and S. Wallon, *ibid.* **B507**, 367 (1997); A. H. Mueller, *ibid.* **B558**, 285 (1999); A. Capella, A. Kaidalov, and J. Tran Thanh Van, Heavy Ion Phys. **9**, 169 (1999).

[5] V. N. Gribov, Zh. Éksp. Teor. Fiz. **57**, 654 (1967) [Sov. Phys. JETP **26**, 414 (1968)].

[6] A. Di Giacomo and H. Panagopoulos, Phys. Lett. B **285**, 133 (1992); A. Di Giacomo, E. Meggiolaro, and H. Panagopoulos, Nucl. Phys. **B483**, 371 (1997).

[7] N. N. Nikolaev and B. G. Zakharov, Z. Phys. C **49**, 607 (1990).

[8] L. L. Frankfurt and M. Strikman, Phys. Rep. **160**, 235 (1988).

[9] K. A. Ter-Martirosyan, Nucl. Phys. **B36**, 566 (1972).

[10] L. P. A. Haakman, A. Kaidalov, and J. H. Koch, Phys. Lett. B **365**, 411 (1996).

[11] J. Bartels, L. L. Frankfurt, and M. Strikman, Phys. Rep. **160**, 235 (1988).

[12] A. Capella, A. Kaidalov, C. Merino, and J. Tran Thanh Van, Phys. Lett. B **337**, 358 (1994); **343**, 403 (1995).

[13] A. Kaidalov and C. Merino, Eur. Phys. J. C **10**, 153 (1999); A. Kaidalov, C. Merino, and D. Perterman, hep-ph/9911331.

[14] A. Capella, A. Kaidalov, C. Merino, D. Perterman, and J. Tran Than Van, Phys. Rev. D **53**, 2309 (1996).

[15] A. B. Kaidalov, L. A. Ponomarev, and K. A. Ter-Martirosyan, Yad. Fiz. **44**, 722 (1986) [Sov. J. Nucl. Phys. **44**, 468 (1986)].

[16] H1 Collaboration, C. Adloff *et al.*, Nucl. Phys. **B497**, 3 (1997).

[17] ZEUS Collaboration, J. Breitweg *et al.*, Phys. Lett. B **407**, 432 (1997).

[18] E665 Collaboration, M. R. Adams *et al.*, Phys. Rev. D **54**, 3006 (1996).

[19] ZEUS Collaboration, J. Breitweg *et al.*, Phys. Lett. B **487**, 53 (2000).

[20] H1 Collaboration, C. Adloff *et al.*, Z. Phys. C **76**, 613 (1997).

[21] ZEUS Collaboration, J. Breitweg *et al.*, Eur. Phys. J. C **6**, 43 (1999).

[22] ZEUS Collaboration, A. Solano, XXXV Rencontres de Moriond QCD and High Energy Hadronic Interactions, Les Arcs, 1999.

[23] H1 Collaboration, C. Adloff *et al.*, Z. Phys. C **74**, 221 (1997).